Article

Highly sensitive and selective photoelectrochemical biosensor for Hg2+ detection based on dual signal amplification by exciton energy transfer coupled with sensitization effect

Ming Zhao, Gao-Chao Fan, Jing-Jia Chen, Jian-Jun Shi, and Jun-Jie Zhu

Anal. Chem., **Just Accepted Manuscript** • DOI: 10.1021/acs.analchem.5b03721 • Publication Date (Web): 24 Nov 2015

Highly sensitive and selective photoelectrochemical biosensor for Hg^{2+} detection based on dual signal amplification by exciton energy transfer coupled with sensitization effect

Ming Zhao [a, 1], *Gao-Chao Fan* [b, 1], *Jing-Jia Chen* [b], *Jian-Jun Shi* [a, b, *], *and Jun-Jie Zhu* [b, *]

[a] School of Chemical Engineering, Anhui University of Science and Technology, Huainan, 232001, People's Republic of China

[b] State Key Laboratory of Analytical Chemistry for Life Science, Collaborative Innovation Center of Chemistry for Life Sciences, School of Chemistry and Chemical Engineering, Nanjing University, Nanjing, 210093, People's Republic of China

ABSTRACT. A highly sensitive and selective photoelectrochemical (PEC) biosensor for Hg^{2+} detection was developed based on the synergistic effect of exciton energy transfer (EET) between CdS quantum dots (QDs) and Au nanoparticles (NPs) coupled with sensitization of rhodamine 123 (Rh123) for signal amplification. First, the TiO_2/CdS hybrid structure obtained by depositing CdS QDs on TiO_2 film was employed as a matrix for immobilizing probe DNA (pDNA). Next, Rh123 was introduced into the pDNA terminal, and then Au NP labeled target DNA (Au-tDNA) was hybridized with pDNA to form a rod-like double helix structure. The detection of Hg^{2+} was based on a conformational change of the pDNA after incubating with Hg^{2+}. In the absence of Hg^{2+}, Rh123 was located away from the electrode surface due to the DNA hybridization, leading

to inhibition of the sensitization effect, and meanwhile the occurrence of EET between CdS QDs and Au NPs resulting in photocurrent decrease. However, after incubating with Hg^{2+}, the rod-like double helix was disrupted and the energy transfer was broken. In this case, the photocurrent recovered, and meanwhile the folded pDNA made the labeled Rh123 move closer to the electrode surface, leading to the formation of the sensitization structure, which evidently increased the photocurrent intensity. The sensitivity of the biosensor for Hg^{2+} detection was greatly enhanced for the dual signal amplification strategy. The linear range was 10 fM to 200 nM, with a detection limit of 3.3 fM. This biosensor provides a promising new platform for detecting various heavy metal ions at ultralow levels.

Keywords: photoelectrochemistry; Hg^{2+} detection; exciton energy transfer; sensitization effect; signal amplification

INTRODUCTION

Exposure to heavy metals, especially mercury, in environmental systems is a critical issue throughout the world. Moreover, mercury is non-degradable, so it can accumulate in plants and animals.[1] The highly toxic ions can be transformed into methyl mercuric compounds, which may be concentrated through biological cycles to cause various diseases, such as pneumonia, enteritis and bronchitis in human beings.[2] Due to high toxicity as well as persistence in the environment and bioaccumulation, mercury species are listed as priority pollutants by many countries and international agencies.[3] Therefore, analytical methods for the trace amount detection of Hg^{2+} are urgently needed. At present, the conventional methods for Hg^{2+} detection include inductively coupled plasma mass spectrometry,[4] cold vapor atomic fluorescence spectrometry,[5] surface enhanced Raman scattering (SERS),[6-8] ultraviolet-visible spectrometry,[9] colorimetry,[10,11] and

fluorometry.[12-14] These methods can facilitate the high sensitivity detection of Hg^{2+} ions,[15] but they still have many drawbacks, such as complex sample preparation procedures, high costs, easy contamination, and non-repeatability. Furthermore, these methods are often hampered by interference from other metals ions. Thus, it is still necessary to develop a more sensitive, selective and economic method for detecting trace amounts of Hg^{2+}.

Photoelectrochemical (PEC) detection is a recent but rapidly developing technique, where light is utilized to excite the photoactive species and photocurrent is employed as the detection signal. PEC method has attracted much attention due to its advantages in terms of higher sensitivity and selectivity compared with conventional methods because of the total separation of the excitation source and detection signal. It also has other advantages, such as uncomplicated devices, low costs, and simple sample preparation. During the past decades, many PEC platforms have been used for detecting biomarkers,[16] DNA sequences,[17] enzymes,[18] and cells[19], but very few for heavy metal ions.[20-23] According to previous studies[24,25], Hg^{2+} can specifically bond with thymine (T) to form a thymine-Hg^{2+}-thymine (T-Hg^{2+}-T) structure, which is even more stable than the Watson-Crick A-T pair. Based on this principle, high selectivity for Hg^{2+} detection can be achieved.

Herein, we developed a novel PEC biosensor for Hg^{2+} detection based on dual signal amplification by exciton energy transfer (EET) between CdS QDs and Au NPs coupled with the sensitization effect of rhodamine 123 (Rh123) to TiO_2/CdS hybrid structure. To fabricate the biosensor, TiO_2 NPs and CdS QDs were modified successively on an indium tin oxide (ITO) slice. Next, probe DNA (pDNA) was immobilized on the electrode via the EDC coupling reaction between carbonyl groups on the surface of the CdS QDs and the amino groups of the pDNA. After Rh123 was introduced into the pDNA terminal via the EDC coupling reaction between the phosphate radical of the pDNA and the amino groups of Rh123, the Au NP labeled

target DNA (Au-tDNA) was immobilized onto the electrode by hybridizing with pDNA to form a double helix structure. The detection of Hg^{2+} was based on the competitive reaction between T-Hg^{2+}-T and the hybridized pDNA with Au-tDNA. Without Hg^{2+}, the photocurrent decreased due to the EET and inhibited sensitization effect. While in the presence of Hg^{2+}, the T-rich pDNA reacted with Hg^{2+}, and the photocurrent evidently increased because of the disrupted EET and formed sensitization structure. This PEC biosensor exhibited high sensitivity, and good specificity, reproducibility and stability. The proposed strategy also provided a general model for the design of PEC biosensors for detecting other heavy metal ions.

EXPERIMENTAL SECTION

Materials and Reagents. ITO slices (type JH52, ITO coating 30 ± 5 nm, sheet resistance ≤ 10 Ω/square) were ordered from Nanjing Zhongjingkeyi Technology Co. Ltd. (China). TiO_2 power (P25) was purchased from the Degussa Co. (Germany). Cadmium chloride ($CdCl_2 \cdot 2.5H_2O$), thioacetamide (TAA), sodium hydroxide (NaOH) and chloroauric acid ($HAuCl_4 \cdot 4H_2O$) were obtained from Shanghai Chemical Reagent Co. (China). Sodium borohydride ($NaBH_4$), 1-ethyl-3-(3-(dimethylamino) propyl) carbodiimide hydrochloride (EDC), N-hydroxysuccinimide (NHS), 3-mercaptopropionic acid (MPA), ethanolamine (MEA), Rh123, poly(diallyldimethylammonium chloride) (PDDA; 20% w/w in water), and tris(2-carboxyethyl)-phosphine (TCEP) were all obtained from Sigma-Aldrich (USA). Ascorbic acid (AA) was purchased from Sinopharm Chemical Reagent Co. Ltd. (China). All other reagents were of analytical grade and used as received. All aqueous solutions were prepared with deionized water (DI water, 18 MΩ/cm), which was obtained from a Milli-Q water purification system. Tris-HCl buffer solution (pH 7.4, 10 mM) containing 0.1 M NaCl was used for preparation and hybridization of DNA stock solutions. The oligonucleotides used in this work were ordered from Shenggong Bioengineering

Co., Ltd. (Shanghai, China) with the following sequences: phosphorylated linker pDNA, 5'-NH_2-$(CH_2)_6$-TTT TTT TTT TTT TTT TTT TTT TTT-P-3'; tDNA, 5'-SH-$(CH_2)_6$-AAA AAA AAA AAA AAA AAA AAA AAA-3'

Apparatus. The morphology and particle size of the samples were characterized by high resolution transmission electron microscopy (HRTEM) (JEOL-2100, Japan). The UV-visible (UV-vis) absorption spectra were obtained on a UV-3600 UV-vis spectrophotometer (Shimadzu, Japan). Photoluminescence (PL) spectra were obtained on an RF-5301PC spectrophotometer (Shimadzu). Electrochemical impedance spectroscopy (EIS) was performed on an Autolab potentiostat/galvanostat (PGSTAT 30, Eco Chemie B.V., Utrecht, Netherlands) with a three-electrode system in 0.1 M KCl solution containing 1.0 mM $K_3[Fe(CN)_6]/K_4[Fe(CN)_6]$ (1:1) mixture as a redox probe, and recorded in the frequency range of 0.01 Hz–100 kHz with an amplitude of 50 mV. PEC measurements were carried out with a homemade PEC system. A 500 W Xe lamp was used as the irradiation source with the light intensity of 400 $\mu W/cm^{-2}$ estimated by a radiometer (Photoelectric Instrument Factory of Beijing Normal University). Photocurrent was recorded on a CHI 660D electrochemical workstation (Shanghai Chenhua Apparatus Corporation, China), and ITO modified electrode, saturated calomel electrode (SCE) electrode, platinum wire were used as working, reference, and counter electrode in this work, respectively. The real sample was tested by atomic fluorescence spectrometry (AFS) (AF-610A, Beijing Rayleigh Analytical Instrument Co., Ltd. China).

Synthesis of CdS QDs. The water-soluble MPA-capped CdS QDs were prepared as described previously with appropriate modifications.[26] Briefly, 172 μL MPA was added to 40 mL of 20 mM $CdCl_2 \cdot 2.5H_2O$ aqueous solution and N_2 was bubbled throughout the solution for 15 min to remove O_2. Next, the pH of the solution was adjusted to 11.0 with 1.0 M NaOH. Then 40 mL 20 mM of TAA solution was added to above solution to obtain MPA-capped CdS QDs, and the

reaction mixture was refluxed under N_2 protection for 2 h at 80 °C. The prepared CdS QDs solution was bright yellow and it was stored in a refrigerator at 4 °C until use.

Preparation of Au NPs. Au NPs were prepared by reducing $HAuCl_4$ with $NaBH_4$, as described previously but with a slight modification.[27] All of the glassware used in the synthesis process was immersed overnight in aqua regia (HNO_3:HCl = 1:3), washed with deionized (DI) water, and then dried. The procedure employed for synthesizing Au NPs was as follows. First, 0.6 mL of ice-cold 0.1 M $NaBH_4$ solution was added to 20 mL of 250 μM $HAuCl_4$ aqueous solution while stirring. The solution immediately became an orange-red color, thereby indicating the formation of Au NPs. The solution was kept in an ice bath for 10 min with stirring. Finally, the solution was reacted at room temperature for another 3 h and the color changed from orange-red to wine red. The prepared monodispersed Au NPs were stored at 4 °C for further use.

Synthesis of Au NP labeled tDNA. The Au NP labeled tDNA (Au-tDNA) was fabricated as described previously.[28] First, TCEP was used to break the S−S bond of the tDNA and 200 μL of tDNA (5 μM) solution was activated by 10 μL TCEP (10 mM) for 1 h. Next, 800 μL of freshly prepared and purified colloid Au NPs was added to the solution. In order to assure the strength of the Au−S bond, the mixture was shaken gently for 16 h, and then centrifuged for 30 min at 16,000 rpm. Finally, the red precipitate was redispersed in 10 mM Tris-HCl. The Au-tDNA solution was stored at 4 °C.

Fabrication of the biosensor. Before preparation, the ITO slices were cleaned by ultrasonic treatment for 15 min in acetone, 1 M NaOH in a water/ethanol mixture (1:1, v/v) and water in order, and then dried at 80 °C for 12 h. Next, a specific amount of TiO_2 powder was ultrasonically dispersed in DI water and 20 μL of this homogeneous suspension was then dropped onto an ITO slice portion with a fixed area of 0.25 cm^2. After air drying, the film was sintered at 450 °C for 30 min in an air atmosphere and then cooled to room temperature. The

PDDA/CdS multilayer film was grown by alternately dipping the ITO/TiO_2 slices into a solution of 1% PDDA and then the as-obtained CdS QDs solution for 10 min, where this coating process was repeated several times. The films were washed carefully with DI water after each dipping step.

pDNA was immobilized onto the ITO/TiO_2/CdS electrode via the classic EDC coupling reaction between carbonyl groups on the surface of the MPA-capped CdS QDs and the amino groups of the pDNA. Specifically, the CdS QDs modified electrode was activated with 20 μL DI water containing 10 mM EDC and 10 mM NHS for 1 h at room temperature, followed by rinsing with Tris-HCl buffer (10 mM, pH 7.4) to remove any excess EDC and NHS. Next, 20 μL of 2 μM pDNA was dropped onto the electrode and it was incubated at 4 °C for 1 h, and then the electrode was rinsed with Tris-HCl buffer to remove unbound pDNA. The dosage of incubated pDNA was excess to ensure the maximum immobilization of pDNA on the electrode surface, and the reason for this is to enlarge the upper limit of detection for Hg^{2+}. After the electrode was incubated with 20 μL of 1 mM MEA for 1 h to block the unbound sites, 20 μL DI water containing 10 mM EDC and 10 mM NHS was used to activate the phosphate radical of pDNA for 1 h at room temperature, and then 20 μL 1 mg/mL Rh123 was dropped on the electrode for 1 h incubation. Rh123 was labeled on the pDNA through the reaction between the phosphate radical of the pDNA and the amino groups of Rh123.[29,30] Subsequently, the electrode was incubated with 20 μL of Au-tDNA for 1 h to allow the hybridization between pDNA and Au-tDNA. After rinsing with Tris-HCl buffer, the electrode was employed as a PEC biosensor and was incubated with 20 μL of different concentrations of Hg^{2+} solutions at 37 °C for 1 h. Finally, the electrode was rinsed with Tris-HCl buffer and prepared for PEC test.

PEC detection. PEC detection was performed at room temperature in Tris-HCl buffer (pH 7.4, 0.1 M) containing 0.1 M AA, which served as a sacrificial electron donor during measurement of

the photocurrent. White light produced by a Xe lamp with a spectral range of 200–2500 nm was utilized as the excitation light, which was switched on and off every 10 s. The applied potential was 0.0 V. The AA electrolyte was deaerated by pumping through pure nitrogen for 15 min before the photocurrent measurement.

RESULTS AND DISCUSSION

Characterization of CdS QDs and Au NPs. Figure 1A shows the UV-vis absorption spectra of the prepared CdS QDs and Rh123. The absorption of the CdS QDs and Rh123 was respectively below 450 nm and 550 nm. The introduction of Rh123 broadened the absorption range of the biosensor, thereby enhancing the utilization of light energy. Overlapping of the spectra between emission band of the CdS QDs and absorption band of the Au NPs is essential for efficient energy transfer. Figure 1B shows the absorption spectrum of the prepared Au NPs and the PL spectrum of the CdS QDs. It can be observed that the absorption peak of Au NPs was located at 512 nm, which was due to the surface plasmon resonance of Au NPs. The emission peak of CdS QDs was located at 550 nm. Apparently, the emission band of the CdS QDs had a considerable spectral overlap with the absorption band of the Au NPs, which affected the subsequent inter-particle energy transfer, thereby reducing the photocurrent response. Figures 1C and 1D displays typical HRTEM images of the CdS QDs and Au NPs, respectively. The lattice fringes of the prepared CdS QDs and Au NPs are clearly visible. The average size of the CdS QDs was about 3.6 nm (Figure 1C) and the diameter of the Au NPs was about 5 nm with a uniform size distribution (Figure 1D).

Optimization of experimental conditions. TiO_2 is a wide energy band gap (~3.2 eV) semiconductor and it could absorb only the ultraviolet light, i.e., less than 10% of the white light, thereby leading to poor utilization of light energy. Compared with TiO_2, CdS has a lower energy

band gap (~2.4 eV) and a higher conduction band edge, which is advantageous for injecting excited electron from CdS to TiO_2. Thus coupling TiO_2 with CdS can extend the absorption wavelength and increase the utilization of light energy. As photocurrent intensity of the biosensor was affected by the concentration of TiO_2 suspension and coating numbers of CdS QDs, the optimal preparation conditions were explored.

The thickness of the TiO_2 film could be controlled by adjusting the concentration of the TiO_2 suspension. To optimize the thickness of the TiO_2 film, different concentrations of TiO_2 suspension were used to prepare ITO/TiO_2/CdS electrodes with six coating numbers of CdS QDs fixed. As shown in Figure 2A, the photocurrent increased as the concentration of the TiO_2 suspension increased from 0.5 to 1.0 mg/mL, but the photocurrent intensity decreased after further increases in the TiO_2 concentration. The electrode fabricated using the 1.0 mg/mL TiO_2 suspension yielded the highest photocurrent. As the concentration increased, more TiO_2 could be deposited on the surface of the bare ITO slice, thereby providing more sites for immobilizing CdS QDs.[31] However, as the TiO_2 concentration increased further, the photocurrent intensity decreased. This may have resulted in diffusion resistance to increased electron motion with further increases in the thickness of the TiO_2 film, thereby leading to a gradual decrease in the photocurrent because surface recombination centers were increasingly available with excess TiO_2.[32] Thus, the optimal concentration of the TiO_2 suspension was 1.0 mg/mL for fabricating the electrode in subsequent experiments.

To optimize the immobilization of CdS QDs, different coating numbers of CdS QDs were used to prepare ITO/TiO_2/CdS electrode. Figure 2B shows the photocurrent intensity of the ITO/TiO_2/CdS electrodes prepared with different coating numbers of CdS QDs. It can be seen that the ITO/TiO_2/CdS electrode with six coating numbers of CdS QDs produced the highest photocurrent. As the coating number increased, the CdS QDs immobilized on the TiO_2 film

gradually increased, thereby leading to more light absorption.[33] With higher coating numbers, excessive CdS QDs immobilization occurred on the TiO_2 film, which offered more surface recombination centers, and the coated PDDA also increased the diffusion resistance to decrease the photocurrent intensity.[34] Thus, six coating numbers of CdS QDs were used in subsequent experiments.

EIS characterization of the biosensor. Electrochemical impedance spectroscopy (EIS) was used to monitor the fabrication process of the biosensor, since it is an effective method for characterizing the interface properties of electrodes. Generally, the impedance spectrum include semicircular and linear parts, where the semicircular part represents the electron transfer limited process at higher frequencies and the linear part is attributable to the limited diffusion process at lower frequencies. The diameter of the semicircle equals the electron transfer resistance (R_{et}), which reflects the electron-transfer kinetics of the redox probe at the electrode interface. Figure 3A shows the impedance spectra obtained from the electrodes formed step by step, where the inset shows the applied equivalent circuit. For ITO/TiO_2 electrode, the circle was quite small (curve a), thereby implying a very small electron transfer resistance, which indicated that $[Fe(CN)_6]^{4-/3-}$ could reach the surface of the bare ITO and exchange the charge rapidly. After the immobilization of CdS QDs, the R_{et} increased greatly due to the hindrance effect of the PDDA polyelectrolytes and the low conductivity of the CdS QDs (curve b). When the ITO/TiO_2/CdS electrode was modified with pDNA, R_{et} increased because of the low conductivity of DNA sequences (curve c). After blocking with MEA, R_{et} decreased (curve d). It was because that MEA reacted with the electronegative carboxyl groups of CdS QDs, which improved the transfer of the negatively charged probe of ($[Fe(CN)_6]^{3-/4-}$).[35] After Rh123 was labeled at pDNA terminal, the R_{et} increased resulting from poor conductivity of Rh123 molecules (curve e). After the electrode was incubated with Au-tDNA, the R_{et} further increased (curve f), implying that the Au-tDNA had

hybridized with pDNA. Accordingly, the EIS characterization suggested successful fabrication of the biosensor.

PEC mechanism of the biosensor. Recently, the energy transfer between semiconductor QDs and metallic NPs has been demonstrated as an advanced and feasible bioassay protocol.[36] Spectral overlap between emission band of the QDs and absorption band of the Au NPs is needed for energy transfer. There was a considerable spectral overlap between CdS QDs and Au NPs, as shown in Figure 1B. In addition, the distance between CdS QDs and Au NPs was also a key factor that affected energy transfer. The distance between the energy donor and the energy acceptor was about (10 ± 2) nm. The length of the designed pDNA sequence in present work was about 9 nm, which was suitable for energy transfer.

Different photoactive species possess different energy band gaps, corresponding to varied optimal absorption ranges for white light. Coupling small band gap photoactive species with large band gap ones to form sensitized structure with stepwise band-edge levels can increase the utilization of light energy and facilitate charge separation, resulting in enhancement of the photocurrent conversion efficiency.[37] In previous studies, many semiconductor materials were used as sensitization agents such as CdS,[38] CdSe,[39] CdTe,[18] and CdSeTe.[40] However, these inorganic sensitization agents have the drawbacks of low light absorption efficiency and poor electrical conductivity. By contrast, very few works employed organic sensitization agents, although they owned advantages of wide adsorption band, high light-absorption efficiency, and many different types of functional groups. In present study, the organic dyes of Rh123 was introduced into the biosensor for signal amplification, because it can broaden the adsorption band and increase the photocurrent intensity due to formation of the sensitization structure.

The biosensor for Hg^{2+} detection was constructed based on the dual signal amplification by exciton energy transfer coupled with sensitization effect. Before incubation with Hg^{2+}, as shown

in Scheme 2A, the pDNA was in a rod-like double helix form. At this time, the exciton energy transfer between CdS QDs and Au NPs occurred, which evidently prevented the photogenerated electrons in the conduction band of CdS from transferring to conduction band of TiO_2, leading to evidently decreased photocurrent intensity. While for Rh123, its sensitization effect to TiO_2/CdS hybrid structure was depressed, because the electron transfer was a distance-dependent process. The detection of Hg^{2+} was performed by the competitive reaction between T-Hg^{2+}-T and the hybridized DNA. Compared with tDNA, Hg^{2+} could react with pDNA to form a more stable folded structure. After incubation with Hg^{2+}, as shown in Scheme 2B, the rod-like double helix was broken and the energy transfer was disrupted, resulting in obviously recovered photocurrent intensity. Meanwhile, after T-Hg^{2+}-T structure formed, the pDNA folded and this forced Rh123 move very close to the surface of the biosensor, which greatly enhanced the photocurrent intensity because of the full generation of the sensitization effect of Rh123.

PEC characterization of the biosensor. The fabrication process of biosensor can also be monitored by the photocurrent response, as shown in Figure 3B. The ITO/TiO_2 electrode yielded an appropriate photocurrent intensity (curve a, I=22.3 μA), because TiO_2 can only absorb the ultraviolet light, resulting in a low photo-to-current conversion efficiency. After CdS QDs immobilization, the photocurrent intensity evidently increased (curve b, I=124.3 μA), which was much higher than the ITO/TiO_2 electrode due to formation of the TiO_2/CdS sensitized structure. The photocurrent decreased after pDNA and MEA immobilization (curve c, I=114.1 μA), which could be explained by weak charge-transfer abilities of both pDNA and MEA. After Rh123 was labeled on pDNA terminal, the photocurrent intensity increased moderately (curve d, I=128.2 μA). That was because the pDNA was in a flexible single-strand form, resulting in partly generation of sensitization effect of Rh123. When Au-tDNA was bound on the electrode by hybridizing with pDNA, the photocurrent intensity decreased noticeably (curve e, I=81.9 μA). In

order to verify that the photocurrent decrease mainly originated from exciton energy transfer between CdS QDs and Au NPs, bare tDNA was utilized to carry out the control experiment. And the comparing results exhibited that the photocurrent decrement to bare tDNA was only about 19.6% of that to Au-tDNA, proving that the exciton energy transfer indeed played a dominate role. After the sensing electrode was incubated with Hg^{2+}, the photocurrent intensity evidently increased due to disruption of the exciton energy transfer and full generation of the sensitization structure (curve e, I=134.3 μA). Thus, all of these results demonstrated the successful fabrication of the PEC biosensor.

PEC detection of Hg^{2+}. The detection of Hg^{2+} was based on conformational change of T-rich oligonucleotides. All of the incubation mixtures had the same volume but contained different concentrations of Hg^{2+}. It was found that the photocurrent response of the sensing electrode was directly related to the concentration of Hg^{2+}. Thus, the photocurrent response was used to detect the concentration of Hg^{2+}. Figure 4A shows the photocurrent response of the biosensor to different concentrations of Hg^{2+}. After incubation with Hg^{2+}, the folded pDNA led to disruption of EET and activation of the sensitization effect of Rh123, thereby yielding gradually increased photocurrent intensity. As shown in Figure 4B, the photocurrent response increased in a linear manner as the logarithm of the Hg^{2+} concentration increased from 10 fM to 200 nM. The regression equation was $I = 96.77 + 7.13 \log C$ (pM), with a correlation coefficient of 0.9923. The detection limit for Hg^{2+} concentration (S/N = 3) was estimated at 3.3 fM. Compared with the previous methods for Hg^{2+} detection, as shown in Table 1, the proposed PEC biosensor exhibited a lower detection limit as well as a wider linear range, demonstrating its superiority.

Reproducibility, selectivity and stability of the biosensor. The reproducibility of the PEC biosensor was assessed based on the relative standard deviation (RSD) for the intra-assay and inter-assay precision. The intra-assay precision was obtained by parallel measuring Hg^{2+} five

times at concentrations of 1 pM, 10 pM, and 100 pM, which yielded a RSD values of 4.5%, 3.6%, and 4.9%, respectively. The inter-assay precision was determined by assaying Hg^{2+} at the same concentration using five sensing electrodes prepared under identical conditions, where the RSD values were 5.2%, 4.8%, and 5.6%, respectively. These results demonstrate the satisfactory precision and reproducibility of this biosensor.

In order to investigate the selectivity of the biosensor, various metal ions such as Ca^{2+}, Zn^{2+}, Cd^{2+}, Mg^{2+}, Mn^{2+}, Co^{2+}, Ba^{2+}, Fe^{2+}, Pb^{2+} and Cu^{2+} were selected for interference test. As shown in Figure 5, the photocurrent responses to Hg^{2+} and to Hg^{2+} involved mixture were very approaching; whereas, the photocurrent responses to other interfering ions were very close to the blank test. These results demonstrated that the proposed biosensor had a satisfactory selectivity for Hg^{2+} detection.

The stability of the designed biosensor was also evaluated. After the biosensor was stored in Tris-HCl buffer (pH 7.4, 10 mM) at 4 °C in a refrigerator for over two weeks, there was no obvious change in the photocurrent response when detecting 100 pM Hg^{2+}, demonstrating good stability of the biosensor.

Tests using a real sample. A fish sample was bought from a supermarket and treated based on a previous literature method with some modifications.[42] Specifically, a certain amount of fish tissue was digested in a mixture containing 8 mL of 18 M H_2SO_4 and 2 mL of 16 M HNO_3 in the Teflon lined stainless-steel autoclave (20 mL) overnight. After 7 mL of 10% H_2O_2 was added to the autoclave, the mixture solution was heated to 160 °C for 4 h and then cool down to the room temperature. The resulting solution was diluted to 50 mL with 10% (v/v) HNO_3 and prepared for AFS and PEC test. The obtained three different concentrations of real samples were analyzed by both atomic fluorescence spectrometry (AFS) and the proposed PEC biosensor. The concentrations of the three real samples measured by AFS were 17.4 nM, 168 pM, and 178 fM,

respectively. While the concentrations of the three real samples measured by the proposed PEC biosensor were (18.3 ± 1.2) nM, (171 ± 8) pM, (173 ± 11) fM, respectively, which were very approaching to the results obtained by the method of AFS. All of the testing results demonstrated that the proposed biosensor was well suitable for the detection of real sample which contained trace amount of Hg^{2+}.

CONCLUSIONS

In summary, we have developed a highly sensitive and selective PEC biosensor for Hg^{2+} detection based on dual signal amplification strategy. The conformational change of pDNA was employed to regulate the occurrence of EET between CdS QDs and Au NPs and sensitization effect of Rh123. In the absence of Hg^{2+}, the EET happened and the sensitization effect was depressed, resulting in low photocurrent intensity. While Hg^{2+} existed, the EET disappeared and the sensitization effect was activated, leading to evidently enhanced photocurrent intensity. Compared with other methods, the proposed PEC biosensor exhibited a low detection limit of 3.3 fM due to cooperation effect of EET between CdS QDs and Au NPs coupled with sensitization of Rh123. This well-designed PEC biosensor also shows great promise for the detection of trace levels of Hg^{2+} in real samples.

AUTHOR INFORMATION

Corresponding Authors

*E-mail: jjshi@aust.edu.cn (J. J. S.); Tel/Fax: +86 554 6668485.

*E-mail: jjzhu@nju.edu.cn (J. J. Z.); Tel/fax: +86 25 83597204.

Author Contributions

[1] M.Z. and G.C.F. contributed equally to this work.

ACKNOWLEDGMENTS

We greatly appreciate the support of the National Natural Science Foundation of China (21020102038, 21335004). We also appreciate the support of the Foundation of Provincial Natural Science Research Project of Anhui Colleges (KJ2014A059) and State Key Laboratory of Analytical Chemistry for Life Science (SKLACLS1418).

REFERENCES

(1) Chung, C. H.; Kim, J. H.; Jung, J.; Chung, B. H. *Biosens. Bioelectron.* **2013**, 41, 827−832.

(2) Zhou, Y.; Zhang, Y. Y.; Pan, F. G.; Li, Y. S.; Lu, S. Y.; Ren, H. L.; Shen, Q. F.; Li, Z. H.; Zhang, J. H.; Chen, Q. J.; Liu, Z. S. *Biosens. Bioelectron.* **2010**, 25, 2534−2538.

(3) Leopold, K.; Foulkes, M.; Worsfold, P. *Anal. Chim. Acta.* **2010**, 663, 127−138.

(4) Bings, N. H.; Bogaerts, A.; Broekaert, J. A. C. *Anal. Chem.* **2010**, 82, 4653−4681.

(5) Angeli, V.; Ferrari, C.; Longo, I.; Onor, M.; D'Ulivo, A.; Bramanti, E. *Anal. Chem.* **2011**, 83, 338−343.

(6) Chen,G. H.; Chen, W. Y.; Yen, Y. C.; Wang, C. W.; Chang, H. T.; Chen, C. F. *Anal. Chem.* **2014**, 86, 6843−6849.

(7) Xu, L. G.; Yin, H. H.; Ma, W.; Kuang, H.; Wang, L. B.; Xu, C. L. *Biosens. Bioelectron.* **2015**, 67, 472−476.

(8) Ma, P. Y.; Liang, F. H.; Diao, Q.P.; Wang, D.; Yang, Q. Q.; Gao, D. J.; Song, D. Q.; Wang, X. H. *RSC Adv.*, **2015**, 5, 32168−32174.

(9) Lorber, K. E. *Waste Manage Res.* **1986**, 4, 3−13.

(10) Yan, W. J.; Wang, Y. L.; Zhuang, H.; Zhang, J. H. *Biosens. Bioelectron.* **2015**, 68, 516−520.

(11) Li, C.; Dai, P. Q.; Rao, X. Y.; Shao, L.; Cheng, G. F.; He, P. G.; Fang, Y. Z. *Talanta* **2015**, 132, 463−468.

(12) Cui, X.; Zhu, L.; Wu, J.; Hou, Y.; Wang, P. Y.; Wang, Z. N.; Yang, M. *Biosens. Bioelectron.* **2015**, 63, 506−512.

(13) Fu, X. C.; Wu, J.; Xie, C. G.; Zhong, Y.; Liu, J. H. *Anal. Methods.* **2013**, 5, 2615−2622.

(14) Wang, G. K.; Lu, Y. F.; Yan, C. L.; Lu, Y. *Sensors. Actuat. B-Chem.* **2015**, 211, 1−6.

(15) Guo, Z.; Liu, Z. G.; Yao, X. Z.; Zhang, K. S.; Chen, X.; Liu, J. H.; Huang, X. J. *Sci. Rep.* **2013**, 1−7.

(16) Fan, G. C.; Han, L.; Zhu, H.; Zhang, J. R.; Zhu, J. J. *Anal. Chem.* **2014**, 86, 12398−12405.

(17) Fan, G. C.; Han, L.; Zhang, J. R.; Zhu, J. J. *Anal. Chem.* **2014**, 86, 10877−10884.

(18) Wang, W. J.; Bao, L.; Lei, J. P.; Tu, W. W.; Ju, H. X. *Anal. Chim. Acta.* **2012,** 744, 33−38.

(19) Zhao, X. M.; Zhou, S. W.; Jiang, L. P.; Hou, W. H.; Shen, Q. M.; Zhu, J. J. *Chem. Eur. J.* **2012**, 18, 4974−4981.

(20) Li, H. B.; Xue, Y.; Wang, W. *Biosns. Bioelectron.* **2014**, 54, 317−322.

(21) Han, D. M.; Jiang, L. Y.; Tang, W. Y.; Xu, J. J.; Chen, H. Y. *Electrochem. Commun.* **2015**, 51, 72−75.

(22) Zang, Y.; Lei, J. P.; Hao, Q.; Ju, H. X. *ACS Appl. Mater. Inter.* **2014**, 6, 15991−15997.

(23) Zhang, B. T.; Guo, L. H. *Biosens. Bioelectron.* **2012**, 37, 112−115.

(24) Ono, A.; Togashi, H. *Angew. Chem. Int. Edit.* **2004**, 43, 4300−4302.

(25) Joseph, J.; Schuster, G. B. *Org. Lett.* **2007**, 9, 1843−1846.

(26) Zhao, W. W.; Wang, J.; Xu, J. J.; Chen, H. Y. *Chem. Commun.* **2011**, 47, 10990−10992.

(27) Zhao, W. W.; Ma, Z. Y.; Yu, P. P.; Dong, X. Y.; Xu, J. J.; Chen, H. Y. *Anal. Chem.* **2012**, 84, 917−923.

(28) Shen, Q. M.; Han, L.; Fan, G. C.; Abdel-Halim, E. S.; Jiang, L. P.; Zhu, J. J. *Biosens. Bioelectron.* **2015**, 64, 449−455.

(29) Zhang, X. R.; Xu, Y. P.; Yang, Y. Q. ; Jin, X.; Ye, S. J.; Zhang, S. S.; Jiang, L. L. *Chem. Eur. J.* **2012**, 18, 16411−16418.

(30) Korri-Youssoufi, H.; Yassar, A. Biomacromolecules. **2001**, 2, 58−64.

(31) Park, N. G.; van de Lagemaat, J.; Frank, A. J. *J. Phys. Chem. B.* **2000**, 104, 8989−8994.

(32) Kuang, D. B.; Ito, S.; Wenger, B.; Klein, C.; Moser, J. E.; Humphry-Baker, R.; Zakeeruddin, S. M.; Gratzel, M. *J. Am. Chem. Soc.* **2006**, 128, 4146−4154.

(33) Chi, C. F.; Lee, Y. L.; Weng, H. S. *Nanotechnology.* **2008**, 19.

(34) Vogel, R.; Hoyer, P.; Weller, H. *J. Phys. Chem.* **1994**, 98, 3183−3188.

(35) Zhao, W. W.; Yu, P. P.; Shan, Y.; Wang, J.; Xu, J. J.; Chen, H. Y. Anal. Chem. **2012**, 84, 5892−5897.

(36) Govorov, A. O.; Bryant, G. W.; Zhang, W.; Skeini, T.; Lee, J.; Kotov, N. A.; Slocik, J. M.; Naik, R. R. *Nano Lett.* **2006**, 6, 984−994.

(37) Lee, Y. L.; Chi, C. F.; Liau, S. Y. *Chem. Mater.* **2010**, 22, 922−927.

(38) Willner, I.; Patolsky, F.; Wasserman, J. *Angew. Chem. Int. Edit.* **2001**, 40, 1861−1864.

(39) Robel, I.; Kuno, M.; Kamat, P. V. *J. Am. Chem. Soc.* **2007**, 129, 4136−4137.

(40) Fan, G. C.; Zhu, H.; Shen, Q. M.; Han, L.; Zhao, M.; Zhang, J. R.; Zhu, J. J. *Chem. Commun.* **2015**, 51, 7023−7026.

(41) Ma, Z. Y.; Pan, J. B.; Lu, C. Y.; Zhao, W. W.; Xu, J. J.; Chen, H. Y. *Chem. Commun.* **2014**, 50, 12088−12090.

(42) Rolfhus, K. R.; Sandheinrich, M. B.; Wiener, J. G.; Bailey, S. W.; Thoreson, K. A.; Hammerschmidt, C. R. *Environ. Sci. Technol.* **2008**, 42, 871−877.

Figures

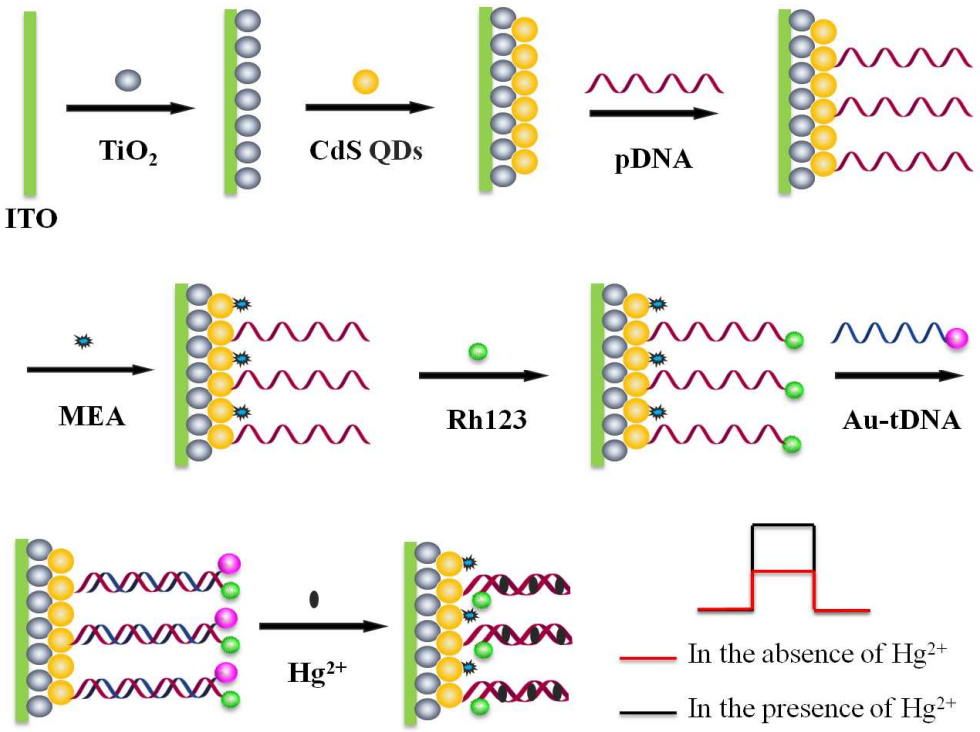

Scheme 1. Fabrication procedure of the PEC biosensor for Hg^{2+} detection.

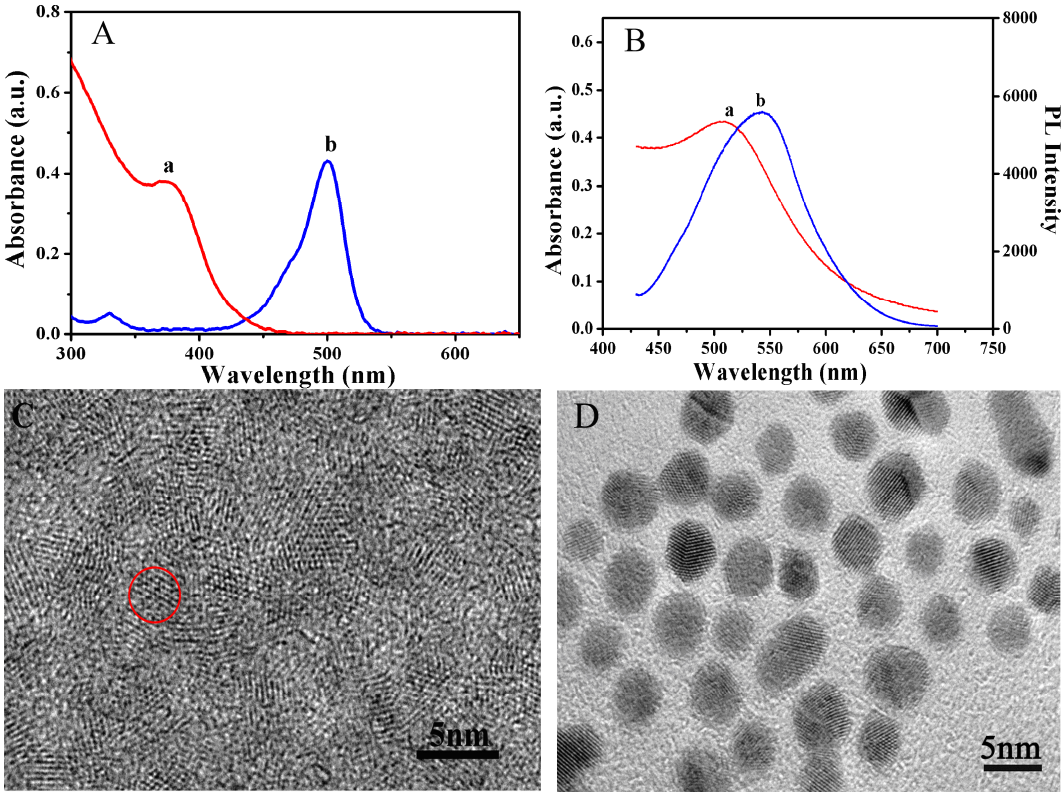

Figure 1. (A) UV-vis absorption spectra of the (a) CdS QDs and (b) Rh123; (B) absorption spectrum of the (a) Au NPs and (b) PL emission spectrum of the CdS QDs; (C) HRTEM image of the CdS QDs; (D) HRTEM image of the Au NPs.

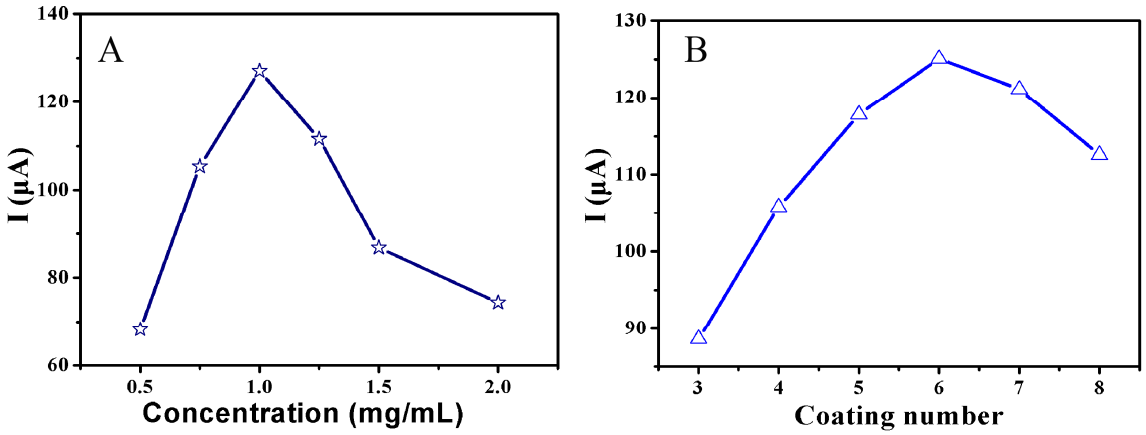

Figure 2. Effects of the (A) concentration of TiO_2 suspension and (B) coating number of CdS QDs on photocurrent responses of the ITO/TiO_2/CdS electrode.

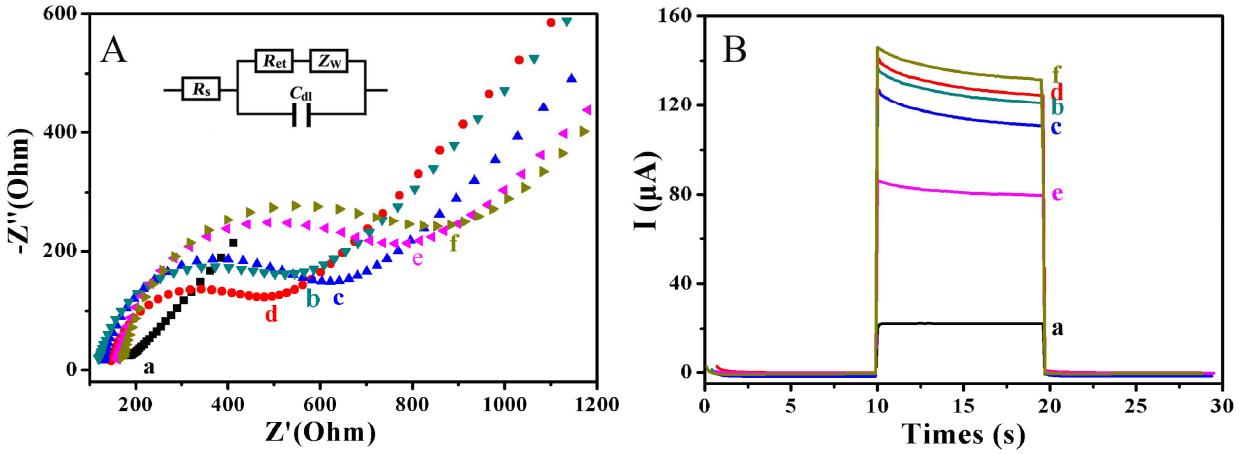

Figure 3. (A) EIS of the (a) ITO/TiO_2 electrode, (b) after CdS QDs immobilization, (c) after pDNA immobilization, (d) after MEA immobilization, (e) after Rh123 labeling, and (f) after Au-tDNA hybridization. The inset in panel A shows the electrical equivalent circuit, where R_s, R_{et}, Z_w, and C_{dl} represent the ohmic resistance of the electrolyte, electron transfer resistance, Warburg impedance, and the double-layer capacitance, respectively. (B) The photocurrent response of the (a) ITO/TiO_2 electrode, (b) after CdS QDs immobilization, (c) after pDNA and MEA immobilization, (d) after Rh123 labeling, (e) after Au-tDNA hybridization, and (f) after the sensing electrode incubated with 20 μL of 2 μM Hg^{2+}.

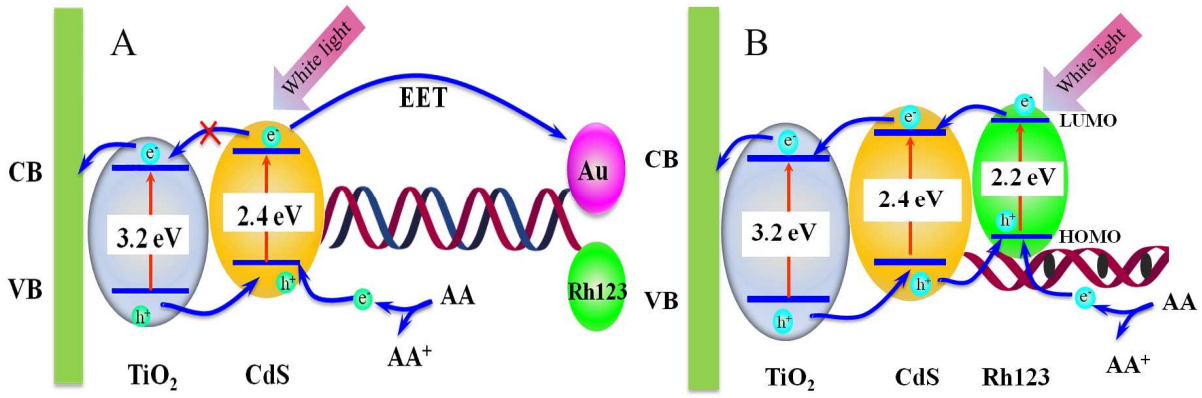

Scheme 2. PEC mechanism of the biosensor (A) before and (B) after incubation with Hg^{2+}.

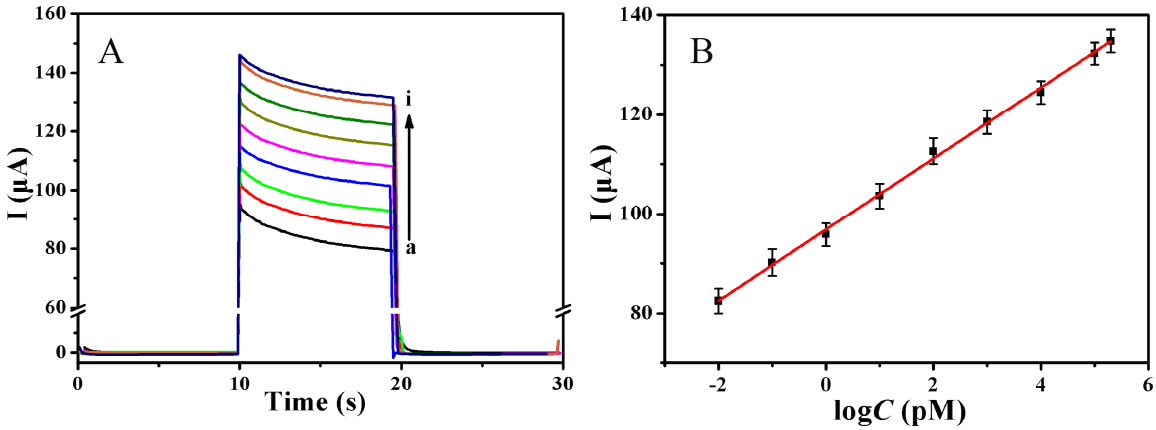

Figure 4. (A) Photocurrent responses of the PEC biosensor to (a) 10 fM, (b) 100 fM, (c) 1 pM, (d) 10 pM, (e) 100 pM, (f) 1 nM, (g) 10 nM, (h) 100 nM, and (i) 200 nM Hg^{2+} detection. (B) Calibration curve of the biosensor. The error bars represent the standard deviations of five replicate determinations.

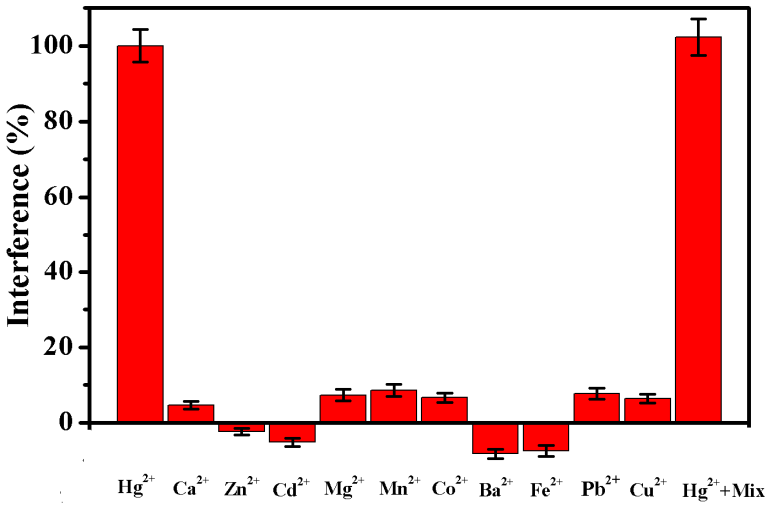

Figure 5. Selectivity of the PEC biosensor for Hg^{2+} detection. The concentration of Hg^{2+} was 100 pM and other interference metal ions was 10 nM. The error bars show the standard deviation of five replicate determinations.

Tables

Table 1. Analytical performance of various methods for Hg^{2+} detection.

Method	Linear range	Detection limit	Reference
SERS	1 pM to 0.1 mM	0.33 pM	8
Colorimetric	1 nM to 30 nM	0.8 nM	11
Fluorescence	20 nM to 90 nM	8 nM	14
PEC	0.1 nM to 10 nM	20 pM	23
PEC	5 pM to 500 pM	1 pM	41
PEC	10 fM to 200 nM	3.3 fM	This study

For TOC only

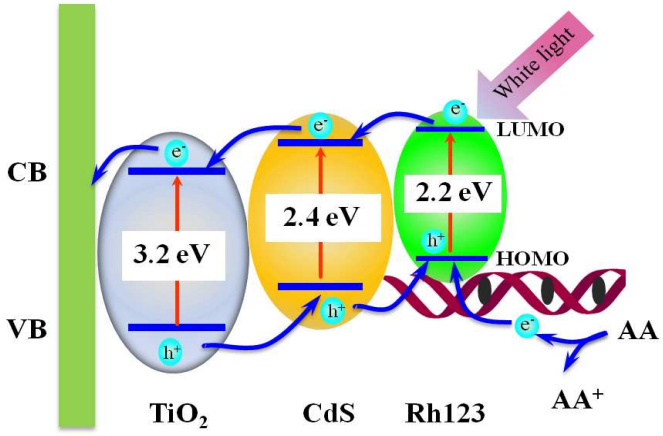
White light
LUMO
HOMO
CB
VB
3.2 eV
2.4 eV
2.2 eV
AA
AA+
TiO2
CdS
Rh123